

WFPC2 Stellar Photometry with HSTphot

Andrew E. Dolphin

National Optical Astronomy Observatories, P.O. Box 26372, Tucson, AZ 85726

Electronic mail: dolphin@noao.edu

ABSTRACT

HSTphot, a photometry package designed to handle the undersampled PSFs found in WFPC2 images, is introduced and described, as well as some of the considerations that have to be made in order to obtain accurate PSF-fitting stellar photometry with WFPC2 data. Tests of HSTphot's internal reliability are made using multiple observations of the same field, and tests of external reliability are made by comparing with DoPHOT reductions of the same data.

Subject headings: techniques: photometric

1. Introduction

With the installation of WFPC2 in December 1993, Hubble Space Telescope (HST) gained an imager capable of high-resolution stellar photometry. This advance provided a number of opportunities, most notably the ability to obtain deep photometry in crowded fields such as nearby galaxies and globular clusters. However, the severely undersampled WFPC2 point spread function (the FWHM is comparable to a PC pixel and about half a WFC pixel) produces a challenge when attempting to obtain accurate stellar photometry. As a result, issues of the number of PSF points calculated per pixel by the photometry software, and of approximations of quantum efficiency variations and charge diffusion, which cause insignificant errors of well under a percent in well-sampled data, contribute significant errors of order a percent in PC data and greater in WFC data.

Because of the vast amount of WFPC2 data available to the astronomical community, HSTphot was developed specifically for its reduction, allowing for the creation of a highly specialized (and efficient) photometry program. The package (*hstphot* and accompanying utilities) runs from the Unix command line, and has been successfully compiled and run on machines running Solaris and Linux. As a manual is available with the package, this paper is intended to describe and test HSTphot rather than to give a detailed explanation of installation and use of HSTphot. Information on obtaining HSTphot can be obtained from

the author by e-mail or from the web. As HSTphot is a continuing project, contributions of improvements, additional utilities, and bug reports and fixes are welcome.

Section 2 gives a description of the HSTphot algorithms, and points out many of the differences between HSTphot and the well-known DAOPHOT and DoPHOT packages. This paper is intended more as a description of the routines and choices that were made for this package and some of its differences with DAOPHOT and DoPHOT, rather than as a detailed description of techniques of stellar photometry. The reader is encouraged to read Stetson’s (1987) introduction of DAOPHOT, which gives a very thorough treatment of this subject. Stetson et al. (1990) and Stetson (1994) present later modifications to DAOPHOT, many of which are also implemented in HSTphot. It should also be noted that few, if any, of the techniques and algorithms used by HSTphot are revolutionary. Rather, I am attempting to provide a photometry package in which the set of choices made is as close to optimal as possible for WFPC2 stellar photometry.

Section 3 of this paper presents a series of tests that were run on HSTphot photometry, examining its photometric and astrometric accuracy. A comparison with a DoPHOT reduction of the same field is also given.

2. HSTphot Algorithms

As a PSF-fitting stellar photometry package, HSTphot is not significantly different in concept from the well-known DAOPHOT (Stetson 1987) and DoPHOT (Schechter, Mateo, & Saha 1993) packages. In order to obtain calibrated photometry for an image, the following steps need to be accomplished:

- Image Preparation
- PSF Determination
- Detection of Stars
- Iterative Photometry Solution
- Aperture Corrections

It is assumed below that the data have had bias, dark current, and flat-field corrections made before beginning this procedure, presumably by the STScI pipeline. The necessary files from the STScI archive for HSTphot are the calibrated data image (*c0f*) and the data quality image (*c1f*). For clarification, utility names are given in *italics* in the following

sections. For example, “HSTphot” refers to the entire photometry package, while “*hstphot*” refers to the specific program that runs the photometry solution.

2.1. Image Preparation

A collection of image preparation utilities is provided with the HSTphot package, which run the necessary processing steps such as masking of bad columns, cosmic ray cleaning, hot pixel masking, etc.

The first preparation procedure is the masking of bad columns and pixels, which is done with the *mask* routine. This simple routine will read the data image (c0f) and the data quality image (c1f) provided by STScI, and proceeds to mask out all pixels that are deemed to be bad - types 1 (Reed-Solomon decoding error), 2 (calibration file defect), 4 (permanent camera defect), 16 (missing data), 32 (other bad pixel), 256 (questionable pixel), and 512 (unrepaired warm pixel). This masking will also eliminate the vignetted region in recent images (very early data quality images do not flag this region). Row 800 and column 800 are also masked out entirely. Because the saturation flag (type 8) in the data quality image is unreliable, all pixels with 3500 or more counts are set as saturated (4095 DN) to avoid ambiguity later in the reductions. All masked pixels are set to the bad data value, -100 DN, and are ignored for the remainder of the photometry.

2.2. Image Cleaning and Combination

The masked image is then ready for cosmic ray cleaning and combination, a process for which the utility *crclean* is designed. This utility uses a routine based on the IRAF task CRREJ, itself a more sophisticated version of the elementary “maximum value reject” method of combining images. *Crclean* is provided a set of images to be combined, which must be taken at the same pointing and with the same filter, and compares the images at each pixel position. All unmasked and unsaturated pixels at that position are scaled for their respective exposure times and compared. The simple procedure would be to use the either median or minimum value of the pixels at a given position as a comparison value (*crclean* provides both options for the user), and reject all values that fall more than

$$\text{max deviation} = \frac{\sigma_{\text{threshold}} \sqrt{\text{Read Noise}^2 + \text{counts}/\text{Gain}}}{\text{Exposure Time}} \quad (1)$$

away from the comparison value. In this equation, Read Noise and counts are both expressed in DN for simplicity, and Gain is expressed in the usual e^- per DN. The value

$\sigma_{threshold}$ is user-defined, and is the maximum number of standard deviations away for which a value should be retained. The recommended value of this parameter is near 3, in other words a 3σ threshold. The pixel values meeting this criterion are then added and scaled to produce an image with an effective exposure time equal to the sum of the individual exposures.

The criterion above makes the assumption that all differences between the images result from shot noise and cosmic rays. In reality, of course, slight image shifts, focus changes, and variability in the objects themselves cause this assumption to be incorrect, and thus a more complex solution is required. All of the additional factors listed will produce a variability between images that scales proportionally with counts rather than with the square root of the counts, and thus such a term is added in quadrature to the threshold,

$$\text{max deviation} = \frac{\sqrt{\sigma_{threshold}^2 \text{Read Noise}^2 + \sigma_{threshold}^2 \text{counts}/\text{Gain} + c^2 \text{counts}^2}}{\text{Exposure Time}}. \quad (2)$$

The constant c is user-defined, with values near 1 providing “safe” cosmic ray cleaning, causing values to be rejected only if they are at least twice the comparison value (this is roughly what is required to avoid chopping the peaks of stars in the case where star is centered on a pixel in one image and centered at the corner of four pixels in another). This extension of the threshold formula is also adapted from CRREJ.

Finally, in the case of poorly-aligned images (by a few tenths of a WFC pixel), there will be a number of stars for which a pixel in one of the images will contain significantly more of the total light than the same pixel in the other images. This happens on the side of the star, where the PSF slope is the steepest. To prevent this from damaging the stellar images, a final additional level of complexity is added, following Saha et al. (1996). The lower allowable limit (comparison value minus the threshold) from the previous paragraph is retained, but the upper limit is modified as follows. Rather than computing a comparison value and threshold from the values of that pixel in all images, these values are instead computed from the maximum values within a 3×3 pixel square centered on that pixel in all images.

A second optional cleaning step can be inserted in the reduction process after the cosmic ray cleaning and background determination (below). This step will attempt to locate and mask hot pixels that were neither flagged by the data quality image nor corrected by the STScI calibration pipeline. Unfortunately, the value of such hot pixels is proportional to exposure time and the count rate is stable between images, so *crclean*, which simply compares the count rate in each pixel with that in other images, will not detect them. This utility, *hotpixels*, is a very simple utility that masks all pixels meeting both of the following criteria. First, the sky-subtracted pixel value is more than ten times the average of adjacent

sky-subtracted pixel values. Second, the sky-subtracted pixel value is more than seven standard deviations above the average value of adjacent pixels. The intent of this utility is not to locate and remove every hot pixel, rather only those that are sitting on blank sky and thus very easy to detect.

As likely clear by the descriptions, both cleaning stages are intentionally cautious in the pixels that are thrown away. Given the very sharp PSFs in the WFC images, this approach seems wise, as a star damaged in the cleaning process is extremely difficult to fix, while most false detections that escape the cleaning process will be identifiable in the photometry output due to unusual χ or sharpness values.

2.3. Background Determination

The sky or background determination is the final mandatory pre-photometry step of HSTphot, and is done with the *getsky* utility. Obviously this is a task that could also be accomplished within *hstphot*, but given the occasional need to re-run *hstphot* with different detection parameters it is preferable to have the sky determined only once. The sky value is calculated at each pixel, using the robust mean of pixel values inside a square “annulus” centered on that pixel. The adoption of the square annulus, rather than the more typical round shape, was made for computational ease (the less multiplication, the faster the program runs). Given that the inner “radius” is sufficiently far from the pixel in question (~ 8 FWHM) that the shape is of little consequence. For the PC, the inner square is 33 pixels on a side and the outer square 45 pixels, thus giving a maximum of 1064 pixels used for the sky determination. The WFC sky calculations use squares of half this size (a 23 pixel outer square and a 19 pixel inner square), with a maximum of 240 pixels used. The robust mean of all unmasked and unsaturated pixels within this area, using a recursive rejection of pixels more than 2.5σ below and 1.75σ above the mean value, is computed. Convergence is determined when a pass rejects no pixels, and the mean sky value from that final iteration is set as the sky value for the pixel. In order to ensure a smoothly-varying background, the sky image is boxcar smoothed to determine the sky values that will be used by *hstphot*.

A few comments regarding the sky calculation process are in order. The sky value can be calculated in one of three ways: a single calculation before the photometry process, a calculation immediately preceding the photometric measurement of a star, and a calculation simultaneous with the photometric measurement. The final choice is the most appealing, as the χ^2 fitting procedure should have little trouble in distinguishing the flat sky from the variable stellar PSF and therefore one can determine the “true” sky value underneath each star with ease. However, as demonstrated by Stetson (1987) and confirmed in my

own similar experiments, the quality of photometry, as measured by the tightness of CMD features, is degraded by this process because of the creation of an additional free parameter. Thus with the third choice eliminated, the HSTphot package gives the option of using the first only or a combination of the first and second. The *getsky* routine determines the *a priori* sky value at each pixel, while *hstphot* can determine a modified sky value for a star immediately before the photometry solution and very close to the star, providing the user two good alternatives for use depending on the condition of the data.

The selection of the sky region involves a tradeoff between three characteristic size scales. The inner radius must be large enough that the star contributes a very small amount of light. The inner “radius” of 9 WFC pixels was chosen with this in mind, although there is still a measurable contribution of light ($\geq 0.007\%$ of the starlight per pixel in the sky region, with the exact amount dependent on the filter and temperature) from the star at this distance. The outer radius must be small enough that the background is either constant or can be fit by a plane over the region used. As most of my own projects involve photometry of field populations in Local Group dwarf galaxies, which have essentially a constant background, I chose to not be concerned with this restriction. However, for the sake of consistency, the PC sky region was set to be exactly twice the size of the WFC annulus, thus creating an identical error in the case of rapidly-varying backgrounds. Finally, the number of pixels within the background region must be much larger than the size of the region used for the photometry solution, so as to minimize the noise caused by the finite sky area. With a maximum photometry area of 81 WFC pixels provided by the PSF library, the 240 pixel sky area ensures that any scatter from the sky calculation will be no more than half the shot noise from the sky inside the photometry region.

Properties of the optional δ sky value that can be determined by *hstphot* (generally most useful for images with a rapidly-varying background) are given below. Use of this technique will tend to mimic DoPHOT sky determinations, which also calculate a sky value extremely close to the star.

2.4. Point Spread Functions

As with DAOPHOT and DoPHOT, *hstphot*’s star brightness and position measurements are made by determining the combination of those parameters that best matches the observed data. Consequently, *hstphot* needs to have a good estimate of the properties of a stellar image before it can begin the photometry. This is aided by the fact that, small focus changes aside, the stellar PSF is consistent in all WFPC2 data taken with the same filter, making it possible to build a library of typical WFPC2 PSFs to be used as initial guesses

when beginning photometry on an image.

Because of the undersampled PSFs, it was decided to calculate the synthetic PSFs for a variety of subpixel centerings, with a spacing of every 0.2 PC pixels (25 total centerings) and 0.1 WFC pixels (100 total centerings). These PSFs were calculated using Tiny Tim PSFs, which were generated with subsampling settings of 0.1 PC pixels and 0.05 WFC pixels for additional resolution. Next, a charge diffusion correction was applied to the Tiny Tim PSF, which was equivalent to smoothing the subsampled PSF with a Gaussian kernel of $\sigma = 0.32$ pixels. (The value of 0.32 pixels was determined by trial-and-error, with this value producing the lowest *hstphot* median χ value for high signal-to-noise data. The value of 0.32 is probably accurate to within 0.05 pixels.) Finally, a subpixel quantum efficiency variation of roughly a 10% efficiency decrease from center to corner was applied, with this value determined in the same way. The choice of the QE fluctuation amount turned out to have very little impact on the quality of the fits, and was thus difficult to determine accurately, with any value between 5% and 15% returning indistinguishable median χ values.

This process was repeated at 64 positions per chip (every 100×100 pixels), thus generating a total of 1600 PSFs on the PC and 6400 PSFs per WFC. Again, it should be noted that the use of Tiny Tim PSFs is not new to HSTphot; CCDCAP (Mighell & Rich 1995), for example, uses Tiny Tim PSFs to determine aperture corrections for small-aperture photometry. However, HSTphot provides what is, to my knowledge, the most elaborate application.

With the grid of PSFs by chip position and subpixel centering calculated, it is worth examining the effect of using these quantized grids rather than an analytic function (such as what is used by DAOPHOT and DoPHOT). It should first be noted that the errors discussed here are of PSF shape rather than the total PSF size. Thus, while a PSF whose total number of counts was in error by 1% would create photometry with an error of 0.01 magnitudes, a PSF whose central pixel was in error by 1% but whose total size was correct would create a much smaller photometric error. The number of counts in a simple χ^2 PSF fit minimization is

$$\text{counts} = \frac{\sum \text{Residual} \times \text{PSF} / \sigma^2}{\sum \text{PSF}^2 / \sigma^2}, \quad (3)$$

which can be simplified to

$$\text{counts} = \frac{\sum \text{Residual}}{\sum \text{PSF}} \quad (4)$$

and

$$\text{counts} = \frac{\sum \text{Residual} \times \text{PSF}}{\sum \text{PSF}^2} \quad (5)$$

for limiting cases of extremely bright stars (in which the noise is dominated by the photon noise of the star) and extremely faint stars (in which the noise is dominated by the constant background and readout noise), respectively. Since the total number of PSF counts is correct, the limiting-case bright star, whose photometric measurement is essentially aperture photometry, is completely unaffected by PSF shape errors. For a limiting-case faint star with a typical WFC PSF with about 35% of the starlight in the central pixel, a PSF shape error in which the central pixel of the model PSF is 1% too bright will create an error of +0.007 magnitudes in the photometry. Because of the PSF^2 term, a similar 1% error involving all four pixels adjacent to the center (which will typically each include 9% of the starlight) would create a magnitude error of just +0.002 magnitudes.

Thus the magnitude errors created by the use of a quantized library of PSFs can be determined based on the errors in the central pixel. The WFC chips, which have the sharpest PSFs and thus are the most likely to show errors, are chosen for this analysis. First, the effect of the 100×100 pixel grid of PSFs is considered. The typical ratio of the central pixel values for diagonally adjacent chip positions is at most 1.016, implying a worst-case 0.8% central pixel PSF error given the lack of any interpolation in the chip positions.

Second, the error from the linear interpolation of PSFs to provide an arbitrary subpixel centering can be estimated. If one compares any PSF in the library to the average of four PSFs diagonal from it, one finds a typical error of 2.8% in the calculated central pixel value. Since linear interpolation errors scale as the baseline squared, this implies a typical central pixel PSF error of 0.7% in the worst-case situation in which the desired position is equally distant from all four nearby library positions.

Finally, there is a very small error when interpolating near the center, created by the fact that Tiny Tim calculates its PSFs centered on the central pixel rather than on the corner of four pixels. As the subsampling factors are 10 on the PC and 20 on the WFC and I therefore chose to combine blocks of 10×10 and 20×20 Tiny Tim pixels to create the library PSFs, the true center of the best-centered PSFs is actually 0.07 pixels off-center in the PC and 0.035 pixels off-center in the WFCs. The effect of this error can be determined by comparing a perfectly-centered PSF to one interpolated from the library, with the error in the central pixel value of the interpolated PSF determined to be 0.3%.

Thus three sources of error in the PSF library can be characterized, and are combined for a worst-case error of 1.8% in the central pixel of the PSF, which will generate an error of 0.013 magnitudes in the photometry of a limiting-case faint star. However, the 1σ scatter in the photometry of the limiting-case faint star will be much smaller, 0.004 magnitudes. Finally, it should be pointed out that our hypothetical limiting-case star actually does not

exist, as the limit of constant noise is only reached if the star has zero counts. Any actual detectable star will contribute some amount to the noise, and thus have a smaller random scatter than the 0.004 magnitudes calculated here. Finally, it is worth reiterating that the brightest stars are unaffected by these considerations.

Within *hstphot*, the PSFs are modified further to compensate for the geometric errors of geometric distortion and the 34th row error. Both of these factors decrease the effective pixel sizes, and thus it is necessary to magnify the PSFs accordingly. The geometric distortion pixel sizes are calculated via the Holtzman et al. (1995a) distortion correction equations; the 34th row error (noted by Shaklan, Sharman, & Pravdo 1995) is characterized by row heights calculated from data supplied by Ron Gilliland. The PSF magnification process is quite simple, with the effective pixel width or height used to determine the fraction of the light from a given row or column that should be moved into the adjacent row or column. To compensate for the fact that the actual PSF value on the outer edge of a pixel is much less than the average PSF value within a pixel, and thus the amount of light transferred should be less, the PC and WFC transfer amounts are multiplied by 0.70 and 0.65, respectively. This value is determined for the typical central pixel, with a worst-case error of a 0.3% in the corrected value of the central pixel, or a maximum magnitude error of 0.002 magnitudes in our hypothetical zero count star. Again, the detailed correction of pixels other than the central pixel are of less interest, given that the PSF² term in the photometric solution will make such errors negligible.

It should be noted that the expansion of PSFs for these geometric errors is a necessity for obtaining accurate PSF-fitting photometry, in addition to the normally-recommended step of multiplying the image by the effective pixel area map (cf Holtzman et al. 1995a). While field-varying PSFs from DAOPHOT or DoPHOT should compensate for the smoothly-varying geometric distortion, the 34th row error needs to be compensated similarly, something which, to my knowledge, is not done in any other photometry package. The use of an uncorrected PSF on an uncorrected image will produce photometry for a star on an affected row in which the shape matches well (thus producing negligible error for faint stars) but the total number of counts detected is 2% too large for bright stars, giving a magnitude error of -0.02 magnitudes. If the data are multiplied by the row size image, the total number of counts are correct (giving correct photometry of bright stars) but the central pixel has an error of 3%, producing a magnitude error of -0.02 magnitudes for the limiting-case faint star. Thus, while the latter case is preferable since the larger random errors should minimize the effect of the systematic +0.02 magnitude shift, in either case one will see a relative error of a few percent between bright and faint stars. Naturally, such an effect only matters significantly for roughly 3% of the stars, but it is my intention that known (and correctable) systematic errors at more than the 1% level be eliminated.

2.5. Star Detection

The star detection algorithm is very similar to that used by DoPHOT (Schechter et al. 1993). After subtracting the sky image from the data image, the residual is scanned for any peaks. Like DoPHOT, a series of passes are made through the image, first for the brightest peaks, then slightly dimmer ones, etc. At the location of any detected peak, an initial guess is made for the central position of the star using the pixel value-weighted averages of the positions of the peak and adjacent pixels,

$$X_{center} = \frac{\sum x_i(R_i - R_{min})}{\sum(R_i - R_{min})} \text{ and} \quad (6)$$

$$Y_{center} = \frac{\sum y_i(R_i - R_{min})}{\sum(R_i - R_{min})}, \quad (7)$$

where x_i and y_i are the X and Y values of the pixels used, R_i is the residual at each pixel, and R_{min} is the minimum residual of any of the pixels used in the centroid calculation.

Using the centroid position as an initial guess, *hstphot* then runs a photometry solution to improve the position and determine the star’s brightness. Rather than running a formal nonlinear least-squares procedure, the photometry solution is determined through an iterative process. At each trial position, a quality-of-fit parameter is determined at the trial position and eight adjacent positions, with a stepsize of 0.2 pixels in the PC and 0.1 pixels in the WFC used to match the spacing of the PSF grid. If the current trial position provides the best fit, the solution is considered converged; otherwise the best fit becomes the new trial position and the process is repeated.

After convergence, if the signal-to-noise (defined in the next section) of the star equals or exceeds the user-defined detection threshold, the star is kept; otherwise it is rejected. As noted above, this is nearly identical to DoPHOT’s star detection procedure, but is significantly different from DAOPHOT’s. DoPHOT and HSTphot both scan the image for stars, and run a photometry solution to determine if the star has a signal-to-noise at or above the threshold value. In contrast, DAOPHOT uses a convolution of the image with a Gaussian of user-defined FWHM to detect locations where stars appear to be. Such a routine will fail in cases in which the PSF FWHM changes significantly over the image and cases in which the background is variable. In either case, the DAOPHOT detection limits will be poorly-defined, with a field-varying PSF causing fewer detections in regions where the FWHM is different from the value used in the convolution and a variable background creating fewer detections over small background and excess detections over high background. Thus the method used by DoPHOT and HSTphot is more robust, providing a more uniform signal-to-noise threshold for the star detections.

As noted in section 2.3, *hstphot* allows the user to either accept the *getsky* sky image or determine a sky value adjustment before each photometry measurement. If the δsky option is used, the sky modification is calculated immediately beyond the photometry radius, at a distance of roughly 5.5 pixels from the star in PC images and 4 pixels in FC images. This value, again calculated using a robust median routine, is subtracted from the residuals during the photometry solution. Because a sky level determined so close to the star will invariably measure some of the starlight as well, the PSFs are also adjusted by subtracting the robust mean in the same region from all PSF values during the photometry solution.

The quality-of-fit parameter that is maximized in the search for the star’s center is based on the detected signal, formal error, and χ determined at each point. These values are defined as follows, calculated over a circular aperture with an effective radius of 3 pixels in the PC and 2 pixels in the WFCs. (These radii contain $\sim 80\%$ of the total starlight, using the encircled energy measurements of Holtzman et al. 1995a.)

$$\text{signal} = \left(\sum_{x,y} R_{x,y} \times PSF_{x,y} / \sigma_{x,y}^2 \times wt_{x,y} \right) / \left(\sum_{x,y} PSF_{x,y}^2 / \sigma_{x,y}^2 \times wt_{x,y} \right), \quad (8)$$

$$\text{error} = \left(\sqrt{\sum_{x,y} PSF_{x,y}^2 / \sigma_{x,y}^2 \times wt_{x,y}^2} \right) / \left(\sum_{x,y} PSF_{x,y}^2 / \sigma_{x,y}^2 \times wt_{x,y} \right), \text{ and} \quad (9)$$

$$\chi^2 = \left[\sum_{x,y} (R_{x,y} - \text{signal} \times PSF_{x,y})^2 / \sigma_{x,y}^2 \times wt_{x,y} \right] / \left(\sum_{x,y} wt_{x,y} \right). \quad (10)$$

$R_{x,y}$ is the residual after subtraction of the sky, $PSF_{x,y}$ is the value of the PSF at the trial chip position and subpixel centering, and $\sigma_{x,y}$ is the expected uncertainty of the measurement at that pixel,

$$\sigma_{x,y}^2 = R_{x,y} + sky_{x,y} + \text{Read Noise}^2. \quad (11)$$

In order to prevent χ^2 from becoming extremely large for bright stars because of PSF errors which cause $R_{x,y} - \text{signal} \times PSF_{x,y}$ to grow proportionally to the star’s brightness, a factor of $c^2 \text{signal}^2 \times PSF_{x,y}^2$ is added to $\sigma_{x,y}^2$ for the determination of χ , with c values of 0.19 in the PC and 0.25 in the WFC providing a median χ near one in the final photometry. This addition is similar to the change from Equation 1 to Equation 2 in the cosmic ray rejection algorithm. Finally, the $wt_{x,y}$ is a weighting factor equal to

$$wt_{x,y} = R_{eff} + 0.5 - \sqrt{(x - x_c)^2 + (y - y_c)^2}, \quad (12)$$

but not allowed to exceed one or drop below zero. R_{eff} is the effective radius (3 PC pixels or 2 WFC pixels), and x_c and y_c are the X and Y positions of the trial position for the star’s center.

Using the calculated signal, error, and χ values, the goodness-of-fit parameter is defined as

$$\text{fit} = \text{signal}/(\text{error} \times \sqrt{\chi^2 + 0.1}). \quad (13)$$

This goodness of fit is essentially the signal-to-noise ratio weighted by $1/\chi$, with the factor of 0.1 added to ensure that the equation does not become infinite should a lucky star be perfectly-fit. The use of this goodness-of-fit parameter rather than a standard χ minimization is to increase the “capture radius,” the maximum error in the centroid position that would permit the star to be located by the photometric solution. If a χ minimization is used, an initial position estimate that falls part way down the side of the star is as likely to slide down the profile and locate the first available peak as it is to climb up the profile to the peak. However, the multiplication by the signal-to-noise will ensure that even if the initial position estimate is well off, the star will be found.

After the entire frame has been searched for stars of all brightness levels, all detected stars are subtracted from the residual image and the process repeated, allowing stars located in the wings of brighter stars to be located. The star list is then cleaned, combining any two stars separated by less than 1.5 pixels, and the photometry solution is begun.

2.6. Solution and Output

The photometry solution runs nearly identically to that of DoPHOT, using an iterative solution. At the start of each iteration, all stars whose neighbors’ photometry was significantly changed in the previous iteration are flagged for solution. “Significantly changed” in this case means that one of the following conditions was true.

- The star’s determined counts was zero.
- The star’s center moved by more than 0.3 PC pixels or 0.15 WFC pixels.
- The photometry changed by more than 1 count and by more than 0.0005 magnitudes.
- The star came within 1.5 pixels of a neighbor and was combined.

The photometry of the flagged stars is then calculated, from the brightest to the faintest, with the procedure described in the previous section used to redetermine the positions and brightnesses. During the solution of a given star, all other stars in the frame are subtracted out. The iterative solution is considered “partially converged” after at least two iterations have run and no stars were eliminated in the previous iteration. After the first iteration in

which this is the case, the PSF residual (described in the following section) is calculated. The solution is considered completely converged after a user-defined maximum number of iterations have run or after no stars are flagged following an iteration.

This solution technique, like the initial star detection process, turned out to be very similar to that used by DoPHOT. However, there are a few significant differences that should be noted. DoPHOT uses a nonlinear χ^2 minimization routine that determines the best position and brightness through a single minimization. HSTphot, on the other hand, maximizes its goodness-of-fit parameter by calculating that value directly at a range of positions. Given that the topology of the search space is well-behaved for a star, such a method is advantageous in that the determination of the goodness-of-fit at a single position is straightforward (using the equations in the previous section) and storing the previous trial fit values in memory will make it trivial to avoid duplicate measurements at the a position. Additionally, the fact that all data are similar allows HSTphot to use a search stepsize that is sufficiently fine to allow good fits while sufficiently large to permit a rapid convergence. The issue at stake is one of efficiency rather than accuracy, with HSTphot reducing data at the same or greater speed than DoPHOT.

An additional difference is seen when comparing HSTphot and DoPHOT with DAOPHOT. While the first two packages share a one-star-at-a-time solution technique, DAOPHOT will solve for all overlapping stars simultaneously. The speed penalty here is considerable, with an order of magnitude difference in running speed between DoPHOT and DAOPHOT reported by Schechter et al. (1993), thus raising the question of whether or not a simultaneous solution of neighboring stars is actually necessary. Given the facts that the cores of WFPC2 PSFs are extremely narrow and that an iterative solution can continue until the faint neighbor stars have converged properly, it would seem that an iterative one-star-at-a-time solution will produce equally good photometry of neighbor stars as will the more sophisticated DAOPHOT method. This assumption is verified through a comparison of HSTphot and DAOPHOT photometry presented by Dolphin (1999) for the WLM globular cluster, as well as a more recent comparison of photometry of the Cassiopeia dwarf spheroidal galaxy presented by Dolphin et al. (1999), with HSTphot producing sharper CMDs with more stars in both cases. Although it is not claimed that the one-star-at-a-time iterative method produces better photometry, these examples demonstrate that it will not significantly hurt the photometry, even in the case of the very crowded WLM globular cluster field.

After convergence is reached or the maximum number of iterations have run, a final photometry iteration is attempted to improve the accuracy. Note that in all previous photometry stages, star positions are only determined at the PSF library grid points (every

0.2 pixels in the PC and 0.1 in the WFCs). In order to improve both astrometric and photometric accuracy, this final iteration determines the best position to the nearest 0.01 pixels, using linear interpolation to compute the PSF at any arbitrary position. As with the previous photometry solutions, this initially involves stepsizes equal to the PSF library grid spacing, but the stepsizes are allowed to contract in this step to provide the more accurate solution.

The *hstphot* output contains the following information: position, counts, sky level, instrumental magnitude, magnitude uncertainty, χ , signal-to-noise, sharpness, and object classification. The signal-to-noise reported here is signal/error as determined in equations 8 and 9, divided by χ if $\chi > 1$ to provide an accurate estimate of the error. This signal-to-noise value is also used in determining the magnitude uncertainty. The instrumental magnitude includes the CTE and zero point corrections that are presented in a companion paper, although the code is included (commented out by default) for the Whitmore, Heyer, & Casertano (1999) CTE corrections.

The reported sharpness is a value which would be zero if the star were perfectly-fit, -1 if it were completely flat, and positive if it were sharper than the typical star. Its definition is

$$\text{sharp} = \frac{\sum_{x,y} (R_{x,y}/\text{signal} - PSF_{x,y}) \times (PSF_{x,y} - \langle PSF \rangle) / \sigma_{x,y} \times wt_{x,y}}{\sum_{x,y} (PSF_{x,y} - \langle PSF \rangle)^2 / \sigma_{x,y} \times wt_{x,y}}, \quad (14)$$

with $\langle PSF \rangle$ being the weighted average of the PSF as defined by

$$\text{sharp} = \left(\sum_{x,y} PSF_{x,y}^2 / \sigma_{x,y}^2 \times wt_{x,y} \right) / \left(\sum_{x,y} PSF_{x,y} / \sigma_{x,y}^2 \times wt_{x,y} \right). \quad (15)$$

Finally, the object classification comes from a comparison of the χ values of fits of the object using the best stellar profile, a single pixel without background (ie, a hot pixel or cosmic ray), and a flat profile (an extended object). If either the cosmic ray or extended profiles provide the best fit, the object is flagged accordingly. Otherwise, one of three star classes is used: a star detected in the first finding pass, a star detected in the second pass and thus likely a close companion of a brighter star, or a star combined from two stars during the photometry process and thus likely a marginally-resolved pair.

2.7. PSF Adjustment

As noted in the previous section, a PSF residual image is calculated for each chip after the first iteration in which the solution is partially converged. This step, which will adjust the library PSFs for the particular focus and tracking conditions of the image being solved,

is necessary because of the implications of equations 4 and 5 - photometry of a bright star depends primarily on the total number of counts in the PSF (which should always be accurate) while that of a faint star depends on the shape of the PSF. In concept, this modification of the library PSFs is similar to the DAOPHOT calculation of a residual used to modify its analytic PSFs. Thus, any error in the PSF caused by the assumption that the library PSFs are correct in every image will have little impact on the bright stars, but the magnitudes of the faint stars will be systematically in error. Stetson (1992) reported systematic errors of up to 0.25 magnitudes over a span of ~ 6 magnitudes in WF/PC data; my own experiments comparing PSF-fitting photometry using unadjusted library PSFs with aperture photometry show deviations of up to 0.15 magnitudes over a similar magnitude range in WFPC2 images, with a typical image showing systematic deviations of 0.05 magnitudes.

Thus it is necessary to calculate a PSF residual image for each frame. A set of stars meeting the following criteria is selected as the set of PSF stars.

- $-0.5 \leq \text{sharp} \leq 0.5$
- $\chi \leq 4$
- The star is more than the PSF radius (6 PC pixels, 4 WFC pixels) away from the edge of the usable chip area
- There are no saturated or masked pixels within the PSF radius of the star.
- No brighter star is within 9 PC pixels or 6 WFC pixels of the star.
- No fainter star with at least half the brightness is within the PSF radius of the star.

The PSF residual is then calculated through an iterative process. First, the average residual around the PSF stars is determined through a robust mean at each point, comparing the residuals around the individual stars (weighted by $1/\text{counts}$, of course). Simply adding the residual to the current PSF, however, will not conserve the number of counts in the PSF, as the mean residual can (and usually will) have a nonzero sum. Since the true PSF should be proportional to the sum of the current PSF and the mean residual, the corrected PSF is set to be

$$\text{new } PSF_{x,y} = c(PSF_{x,y} + R_{x,y}), \quad (16)$$

where $R_{x,y}$ is the mean residual at the point and c is a constant chosen to conserve the PSF size,

$$1/c = 1 + (\sum x, y R_{x,y}) / (\sum x, y PSF_{x,y}). \quad (17)$$

After each modification of the PSF in the iterative process, the photometry of all PSF stars and their neighbors is recalculated. This process continues until convergence is reached, with convergence defined by no PSF point being changed by more than $\sim 0.1\%$ of the total starlight. Typically, the adjustments made to the library PSFs are small, with the central pixels adjusted by less than 3% of the total starlight, indicating FWHM changes of $\sim 9\%$, assuming that a typical central pixel contains 34% of the total light. In a typical trial image, the addition of the PSF residual image reduced the median χ values by 6%.

2.8. Aperture Corrections

The final step necessary to have properly calibrated photometry is to determine and apply aperture corrections, the average difference between aperture photometry with a 0.5 arcsec radius used by H95 and the PSF-fitting magnitudes determined by *hstphot*. It should be noted that, since the Tiny Tim PSFs are calculated with a 0.5 arcsec radius and normalized to a total PSF value of 1.0, and since the total PSF brightness is conserved in both the PSF calculations and in the PSF residual calculation, the application of aperture corrections should not be necessary in theory. This is actually close to the truth in practice as well, with aperture corrections in fields with a constant background and bright, well-separated stars generally being no more than a few hundredths of a magnitude. This provides the luxury of the user being able to omit the aperture corrections altogether in cases where a lack of bright, isolated stars would produce aperture corrections uncertain by more than this amount.

The utility provided for this task is *getapcor*, which identifies up to a user-defined number of good stars in each image with more than a user-defined minimum number of counts. The selection criteria for these stars are similar to those for PSF stars, and are listed below.

- Must have been classified as a star
- $-0.5 \leq \text{sharp} \leq 0.5$
- $\chi \leq 2.5$
- At least 0.75 arcsec from the edge of the field or any saturated or masked pixels
- At least 0.75 arcsec from any brighter star

All stars that meet these criteria have the number of counts falling within the 0.5 arcsec aperture calculated, with each value decreased by a sky value determined in the annulus

from 0.5 to 0.75 arcsec from the star. The aperture correction for the star is simply

$$\Delta mag = -2.5 \log\left(\frac{C_{aperture}}{C_{hstphot}}\right), \quad (18)$$

where $C_{aperture}$ and $C_{hstphot}$ are the counts within the aperture measured by *getapcor* and the counts measured by *hstphot*, respectively. Another robust mean routine is used to determine the overall aperture correction for each chip, based on the Δmag values for all of the aperture stars.

2.9. Multiphot

A recent addition to the HSTphot package is *multiphot*, a program designed to simultaneously solve multiple images in a single run. Again, this concept is far from new, and is to *hstphot* what ALLFRAME (Stetson 1994) is to DAOPHOT. The primary advantages in using *multiphot* rather than *hstphot* are that it is easier to compensate for bad pixels or cosmic rays that are only in one image and that a more accurate photometric solution is obtained by reducing the number of free parameters per star from $3 \times N_{images}$ (X, Y, and counts in each image) to $2 + N_{images}$ (global X and Y positions and counts determined in each image). However, there is somewhat of a tradeoff involved - in order to prevent *multiphot* from using too much memory (*hstphot* allocates about 20 Mb per image), some simplifications had to be made, along with the use of 32-bit floating point rather than 64-bit. The simplified photometry, which affects the expected noise at each pixel, increases uncertainties by roughly 0.005 magnitudes for bright stars, while the increased roundoff error contributes another 0.002 magnitudes of uncertainty. Given a limiting accuracy of about 0.011 magnitudes determined for *multiphot*, these uncertainties will contribute little to the overall error budget.

Overall, the *multiphot* algorithms are nearly identical to those in *hstphot*. The only significant exception is the necessary one: when determining the goodness-of-fit of a trial position, a combined signal, error, and χ are used instead of just the values from a single image. (All PSF information is separate for the exposures, of course, with a different residual image calculated for each image being reduced.) However, there are a few additional complexities that must be addressed by *multiphot*.

The most significant additional problem faced by *multiphot* is that the images need to be properly aligned. To ensure accurate PSF-fitting magnitudes, the accuracy needs to be accurate to at least 0.1 WFC pixels. Thus the alignment issue requires a correction for geometric distortion (which increases the offsets between two images by up to 2% at

the corners compared with the center), the filter-dependent plate scale (which causes a shift of ~ 0.4 pixels between F555W and F814W positions in the corners), and of course an overall shift. The Holtzman et al. (1995a) distortion equations are adopted to determine the change in the offset as a function of position, while the overall shift in X and Y can be easily determined by *multiphot* through a comparison of star positions on the two frames. No rotation is solved for, nor is any necessary in fields that I have examined with *multiphot*.

The filter-dependent plate scale changes are more difficult to correct. Initially, the Trauger et al. (1995) wavelength-dependent distortion corrections were used to correct for both this and the geometric distortion, but this proved to be inadequate. Thus it was necessary to use the empirically-determined Holtzman et al. (1995a) distortion correction (which was calculated for F555W) and to determine the filter-dependent corrections empirically, something that was done by examining archival images of the Omega Centauri standard field taken in all 19 HSTphot filters (except for F170W). The F170W correction was determined from other archival data. The form of the corrections was adopted from fits to the Trauger et al. (1995) correction equations, despite the known errors, for lack of any better source of information.

$$X_{filt} = (X_{F555W} - 400) \times c_{filt} \times [1 + 7 \times 10^{-7} * ((X_{F555W} - X_c)^2 + (Y_{F555W} - Y_c)^2)] + 400, \quad (19)$$

and

$$Y_{filt} = (Y_{F555W} - 400) \times c_{filt} \times [1 + 7 \times 10^{-7} * ((X_{F555W} - X_c)^2 + (Y_{F555W} - Y_c)^2)] + 400. \quad (20)$$

X_{filt} and Y_{filt} are the X and Y positions in any filter, X_{F555W} and Y_{F555W} are the positions of the same star on an F555W image, c_{filt} is the filter-dependent term and values are given in Table 1, and X_c and Y_c are roughly equal to 384 on the PCs and 394 on the WFCs.

Finally, in order to provide a meaningful combined count total, it is necessary for *multiphot* to determine apply aperture corrections to the count rates from the individual images. This is done with a routine nearly identical to *getapcor*, except that it is more forgiving of bad points in the wings of the stars. (Given a set of many exposures, it would likely be impossible to find any good PSF stars that were completely free from bad pixels in all images.)

The output from *multiphot* is identical in format to that from *hstphot*, except that the photometry information is listed individually for all frames processed, as well as combined photometry provided for every filter that was included.

3. Tests of HSTphot

An F555W WFC2 image of IC 1613 is displayed in Figure 1, with the detected stars and cosmic rays subtracted from half the image in order to provide an initial “sanity check” on HSTphot. (Note that the white lines and dots are the masked bad columns and hot pixels, not residuals.) In general, *hstphot* appears to be treating objects as it should. The galaxies are left alone, aside from what are either foreground stars or clusters or HII regions in the galaxies, which indicates that the object classification scheme in *hstphot* is working properly.

The stellar residuals themselves also provide a sanity check. The lack of similar features in the bright residuals is evidence that the average PSF is correct, and that the PSF residual image was correctly determined. The lack of monopole residuals in the stars likewise indicates proper PSF width and star brightness determinations. The lack of dipole residuals (highly positive on one side and highly negative on the other) is indicative of proper centering. Although this is certainly not a quantitative test, it gives evidence that, at the very least, HSTphot isn’t completely off target in its methods. More detailed (and quantitative) comparisons follow in the next sections.

3.1. Photometric Reliability

In order to determine whether or not HSTphot photometry is reliable, a comparison was made between photometry of eight combined 2400s F555W images of a field in IC 1613. The data were taken with four dithering positions, essentially providing four independent sets of observations of the same field. (In fact, it should be noted that the dithering provides something of a worst-case comparison, as stars centered in one image are on the edge or corner in the others.) The data were processed in the standard way, with each image combined from two 1200s images for cosmic ray removal, and run through HSTphot independently. (Note that *Multiphot* could have been used to produce more accurate photometry, but the resulting photometry would not have been completely independent.)

The results of the comparisons between the fields are shown in Figure 2, with a 1σ line plotted through the data. *Hstphot* uncertainties for the points are shown for comparison in the bottom panel. The *hstphot* uncertainties match the measured 1σ uncertainties well, except at the bright end where there appears to be a minimum error of 0.027 magnitudes. Part of this error is due to the assumption that none of the stars in these data are variable, which is incorrect. After running a variable star analysis and retaining only the stars that are apparently non-variable, the minimum error in the HSTphot photometry drops to 0.02

magnitudes. If using *multiphot*, the reduced number of free parameters in the photometric solution decreases the error further, with a minimum of image-to-image scatter of 0.01 magnitudes observed, consistent with Stetson’s (1998) result in his CTE solution.

3.2. Astrometric Reliability

Although HSTphot was not designed to produce precision astrometry, its fairly careful treatment of PSFs provides accurate stellar position measurements. The data used in the previous section can also be used to test HSTphot’s astrometric accuracy. This was first attempted by simply removing the Y offsets from the 34th row error, applying the Holtzman et al. (1995a) geometric distortion equations and applying a global offset for each star. The results are shown in Figure 3, with a limiting astrometric accuracy of ~ 10 mas for the bright stars. This scatter is largely from the use of a global offset, rather than independent offsets for each chip, and reflects astrometric uncertainties in attempting a single astrometric solution for all four chips.

As Anderson & King (1999) have demonstrated, high-precision astrometry can be made by comparing star positions to a grid of nearby bright stars. Making a similar comparison with the HSTphot data significantly improves the quality of the astrometry. Results are shown in Figure 4, with the limiting astrometric accuracy reduced to 0.05 pixels in each chip (2.5mas in the PC and 5.4mas in the WFCs). This value, which corresponds to 0.03 pixel accuracy in both X and Y directions, is similar to values quoted by Anderson, King, & Meylan (1998). Given that the PSF library is only calculated with resolution of 0.2 pixels in the PC and 0.1 pixels in the WFCs and are interpolated to intermediate values, this accuracy is surprisingly good and could presumably be improved further if a finer grid of PSFs were calculated.

3.3. Object Classification

The classification of non-stellar objects is critical to obtaining accurate stellar photometry, as such objects would otherwise contaminate the CMD. Three columns of the *hstphot* output are useful in classification. First is an object type, as described in Section 2.5. It is a safe assumption that all objects determined to be non-stellar should be omitted. The residual shown in Figure 1 omits extended objects, and subtracts cosmic rays (single pixels) as such rather than as stars.

The second useful column is the object’s sharpness, also defined in Section 2.5. Figure

5 shows all objects in one of the IC 1613 images, with cosmic rays and extended objects (as determined by *hstphot* via object type determination) plotted with circles and squares. The “stars” well above the principal trend (at sharpness ≥ 0.4) are multi-pixel cosmic rays, which were not identified by *hstphot* since its cosmic ray model is a single pixel. In general, requiring a sharpness between -0.3 and +0.3 should reject most cosmic rays and extended objects that were not classified by *hstphot*, while retaining most of the stars.

Finally is the χ column, which simply gives the quality of the fit. The bottom panel of Figure 5 shows all objects, with χ plotted against counts. The unidentified cosmic rays seen in the sharpness plot are also seen here, with χ values of greater than 3 or 3.5, and either limit thus useful for eliminating false detections. The use of other poorly-fit stars depends on the quality of the data and the application.

These plots permit the determination of selection criteria for *hstphot* output. If one needs a complete CMD, a χ threshold of 3 should keep most of the stars, but if a clean CMD is preferable a χ threshold of 1.5 will eliminate most detections. The χ limit should be relaxed in the case of very crowded images, such as what is seen in star clusters and in the denser regions of Local Group galaxies. A plot similar to that given in the bottom panel of Figure 5 will quickly determine the appropriate cutoffs for any given situation.

3.4. Comparison With DoPHOT

Comparison photometry on one the WFC2 chip of one of the IC1613 images was provided by Jennifer Christensen using DoPHOT, as described by Saha et al. (1996), with aperture corrections and calibration but the no CTE or zero point corrections applied. Likewise the *hstphot* magnitudes were given aperture corrections but no CTE or zero point corrections. Given that HSTphot is somewhat of a black box with very few adjustable parameters, my photometry using HSTphot is probably identical to what anyone else would obtain. The DoPHOT photometry package was run in the manner prescribed by Saha et al. (1996). As this method is optimized for Cepheid studies and thus uses a background region very close to the star, the δ sky option was used in the HSTphot reduction as well to avoid an inherent advantage given to HSTphot by the use of a larger sky region.

The differences between the HSTphot and DoPHOT F555W and F814W magnitudes are shown in Figure 6, and show no significant differences. Overall, the median difference is +0.001 magnitudes, with a slight (0.01 magnitude) difference in the individual filters that is comparable to the uncertainty in the HSTphot aperture corrections and thus not significant. The respective CMDs are also shown in Figure 7, with the HSTphot CMD a

few hundredths of a magnitude narrower in most places and containing significantly fewer bad points (such as the “stars” to the red of the red giant branch). Table 2 shows the average and scatter in F555W-F814W values for two regions of the comparison CMDs - the upper RGB (~ 20 stars) and the red clump (~ 400 stars) - with HSTphot returning the sharper feature in both cases. Unfortunately, the low signal-to-noise does not permit a meaningful comparison of the main sequence and lower RGB regions, with scatter photon noise alone being >0.1 magnitudes and will thus dwarfing any minor differences caused by the photometry programs.

4. Discussion

A new photometry package, HSTphot, has been developed specifically for the challenges of reducing WFPC2 data. Although HSTphot borrows many of its concepts from previous reduction software, its focus on addressing one specific problem provides for the development of a package that reduces WFPC2 data very efficiently and accurately. A second program, *multiphot*, is also briefly described. This program applies modified HSTphot routines to multiple images in order to run photometry simultaneously. This program will likely be the most useful in the end, although it is newer and thus has not seen as much use (and received as much testing) as *hstphot*. As noted in the introduction, a manual is provided with the HSTphot package, and contains instructions for installation of the package, preparing the data, and running *hstphot* and *multiphot*.

Tests of HSTphot produced encouraging results about its photometric and astrometric reliability. A test of the residuals showed that *hstphot* fits PSFs, centers stars, and measures brightnesses correctly. It appears to have a limiting external (image to image) photometric accuracy of ~ 0.02 magnitudes, and an astrometric accuracy of ~ 0.05 pixels in position (0.03 pixels in X and Y). A comparison with DoPHOT reduction of a field showed no systematic differences, although HSTphot returned a cleaner CMD with less scatter in the major features and fewer obviously bad points.

One significant advantage in using a package designed specifically for WFPC2 is that HSTphot runs with almost no user interaction required. This is possible because the number of chips, vignetted regions, rough PSF sizes, etc. are the same in every image. This specialization has two benefits. First is that the HSTphot routines are optimized for WFPC2 data, and thus run quickly. Second is that because many of the parameters are predetermined, HSTphot requires minimal user input and can be run easily in batch mode. For example, for the CTE study that I made using HSTphot, the entire 1000+ images of Omega Centauri and NGC 2419 were reduced at a rate of about 7.5 minutes per image,

including sky calculation, aperture corrections, and alignment. This speed is comparable to the rate at which the STScI archive provided the data. HSTphot is also being used by the HST Snapshot Survey of Nearby Dwarf Galaxy Candidates (Seitzer et al. 1999) to provide uniform photometry of the sample of galaxies, as well as by other users.

I would like to thank Jennifer Christensen for providing the DoPHOT comparison photometry and Ron Gilliland for providing the data used for the 34th row correction. I would also like to thank Dan Zucker and Ted Wyder for help with debugging HSTphot and facilitating the port to linux. This work was supported by NASA through grants GO-02227.06-A and GO-07496 from Space Telescope Science Institute.

REFERENCES

- Anderson, J., & King, I. R. 1999, *PASP*, 111, 1095
- Dolphin, A. E. 1999, PhD thesis, University of Washington
- Dolphin, A. E. et al. 1999, AAS meeting 195, 08.04
- Holtzman, J. et al. 1995a, *PASP*, 107, 156
- Holtzman, J. et al. 1995b, *PASP*, 107, 1065
- Mighell, K. J., & Rich, R. M. 1995, *AJ*, 110, 1649
- Saha, A., Sandage, A., Labhardt, L., Tammann, G. A., Macchetto, F. D., & Panagia, N. 1996, *ApJ*, 466, 55
- Schechter, P. L., Mateo, M., & Saha, A. 1993, *PASP*, 105, 1342
- Seitzer, P. et al. 1999, AAS meeting 195, 08.01
- Shaklan, S., Sharman, M. C., & Pravdo, S. H. 1995, *Appl. Opt.*, 34, 6672
- Stetson, P. B. 1987, *PASP*, 99, 191
- Stetson, P. B. 1992, in *Astronomical Data Analysis Software and Systems I*, eds. D. M. Worrall, C. Biemesderfer, & J. Barnes, ASP Conference Series, 25, 297
- Stetson, P. B. 1994, *PASP*, 106, 250
- Stetson, P. B. 1998, *PASP*, 110, 1448
- Stetson, P. B., Davis, L. E., & Crabtree, D. R. 1990, in *CCDs in Astronomy*, San Francisco: ASP, p. 289

Trauger, J. T., Vaughan, A. H., Evans, R. W., & Moody, D. C. 1995, in *Calibrating Hubble Space Telescope: Post Servicing Mission*, ed. A. Koratkar & C. Leitherer, Baltimore: STScI, p. 379

Whitmore, B., Heyer, I., & Casertano, S. 1999, *PASP*, 111, 1559

Fig. 1.— F555W WFC2 image of IC 1613, with stars subtracted from the left half

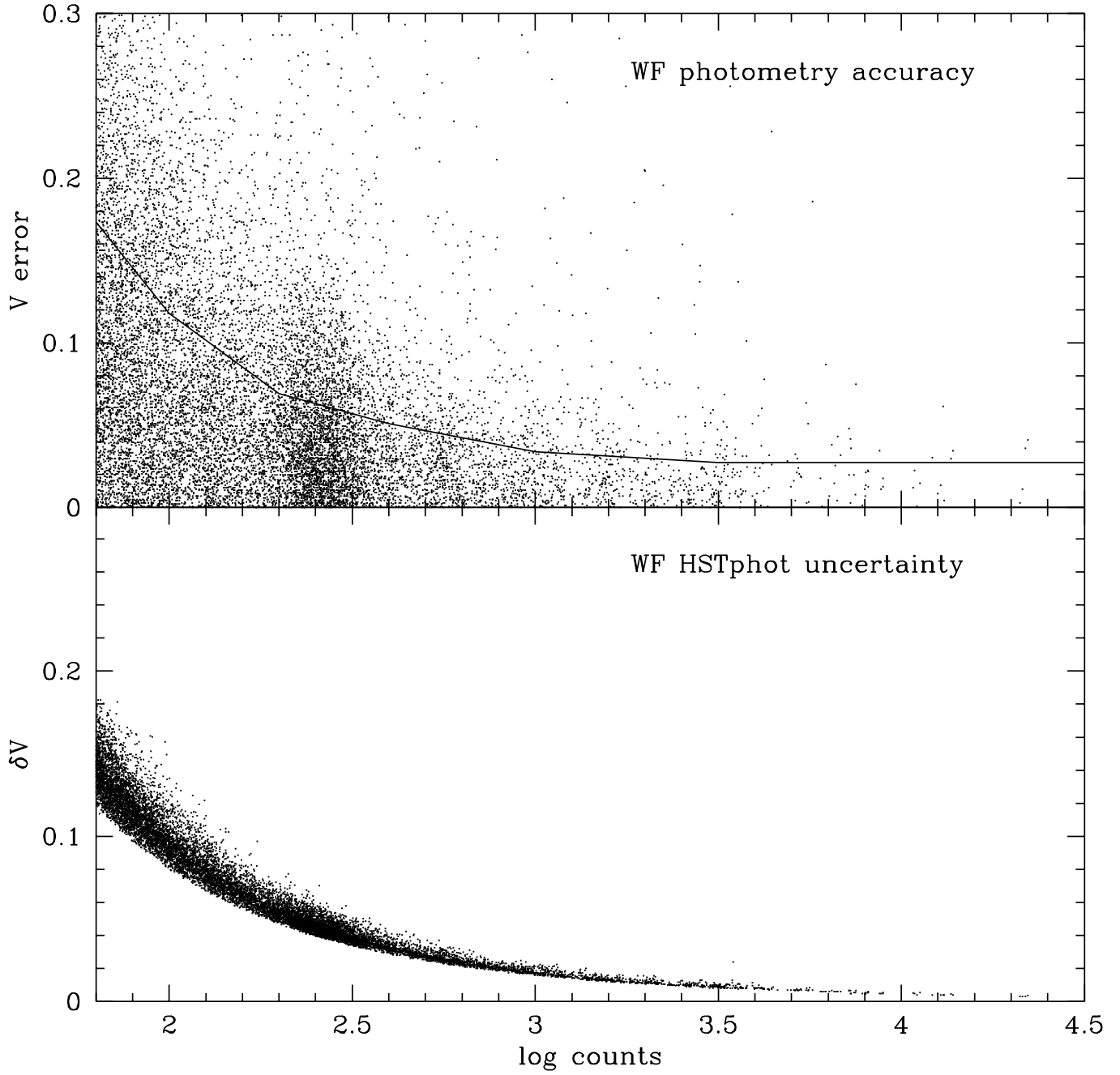


Fig. 2.— Photometry error, based on repeated F555W observations of the IC 1613 field

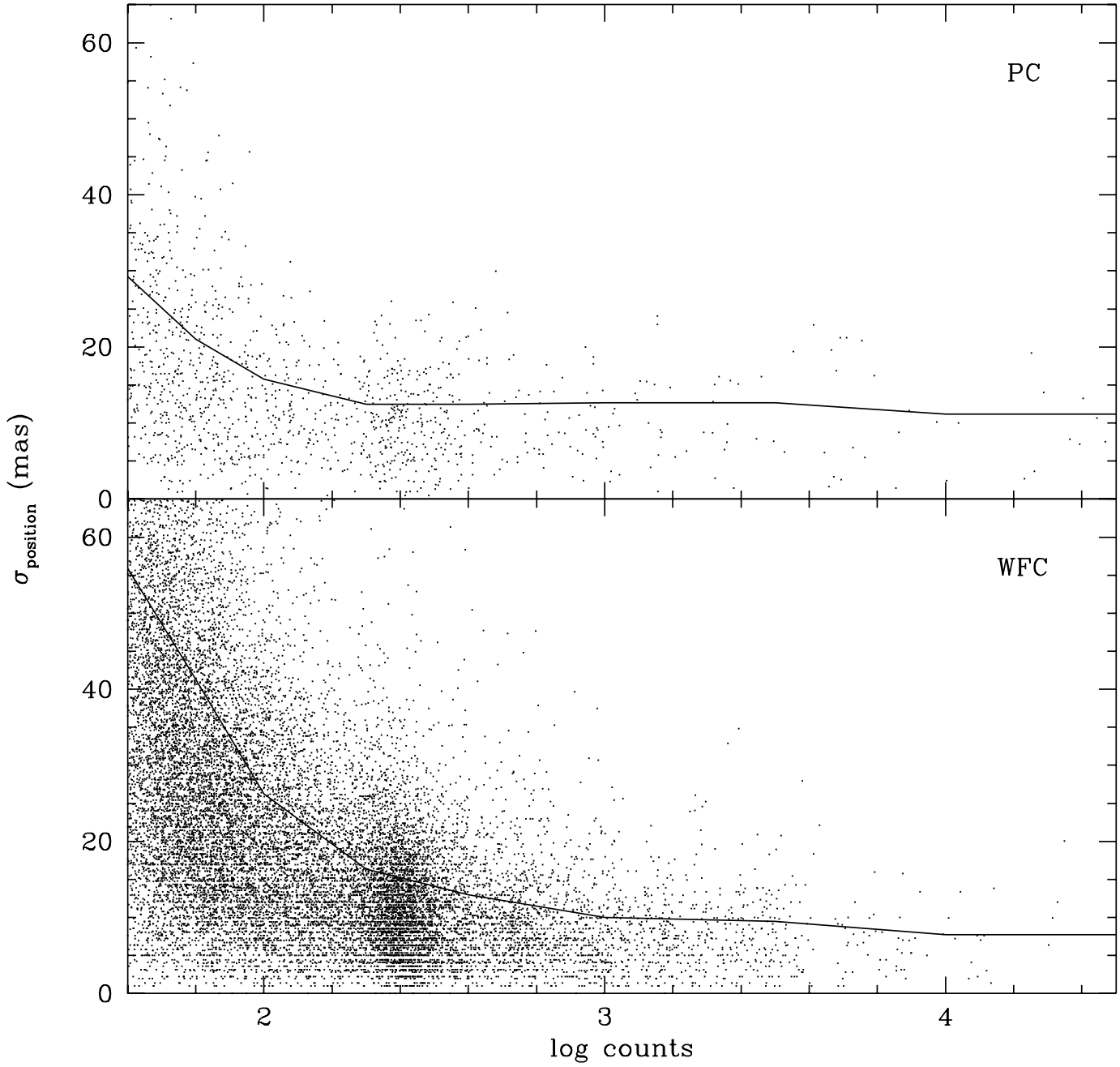


Fig. 3.— Astrometry error, based on a global astrometry solution

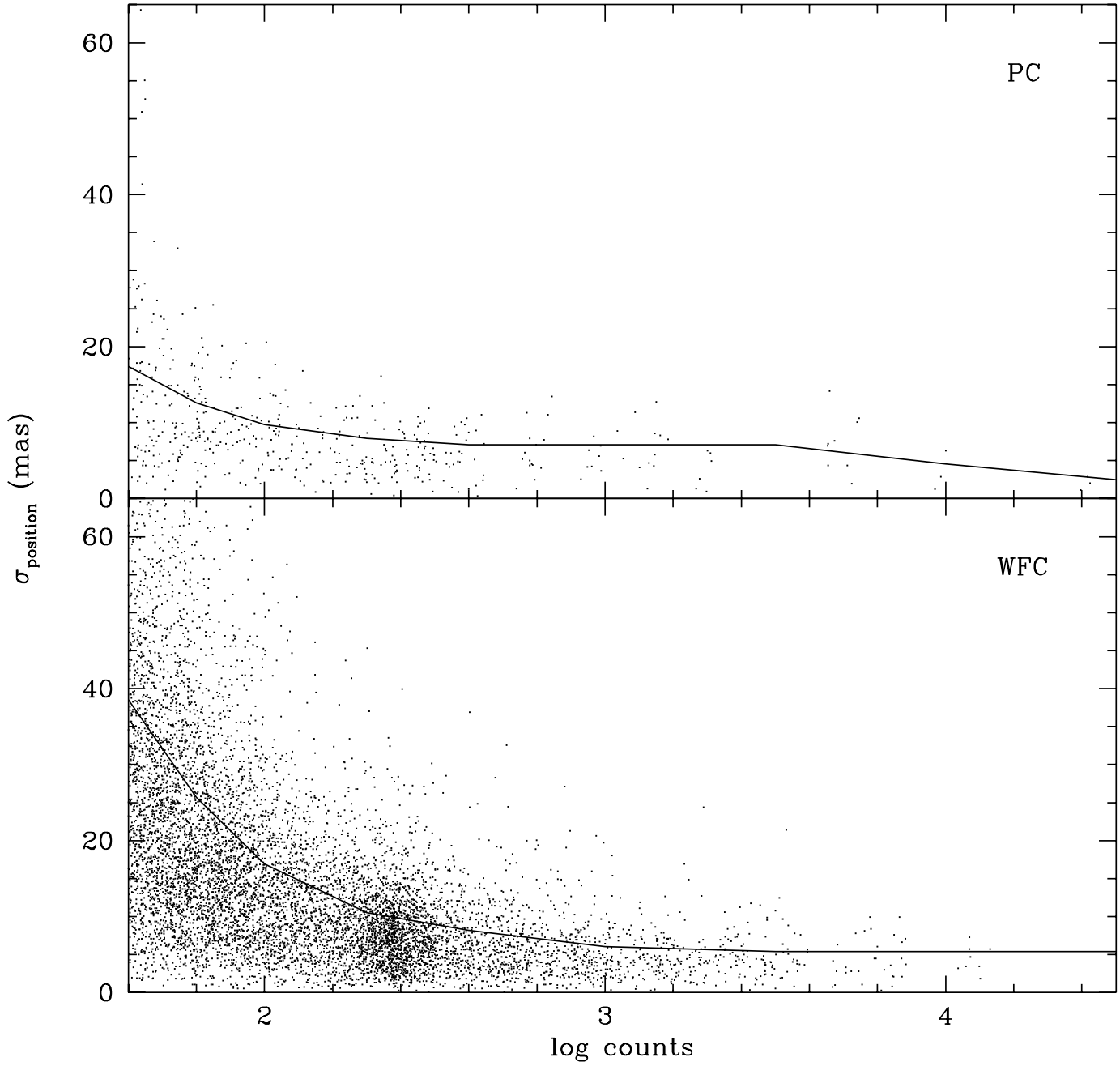


Fig. 4.— Astrometry error, based on positions relative to a grid of bright stars in each image

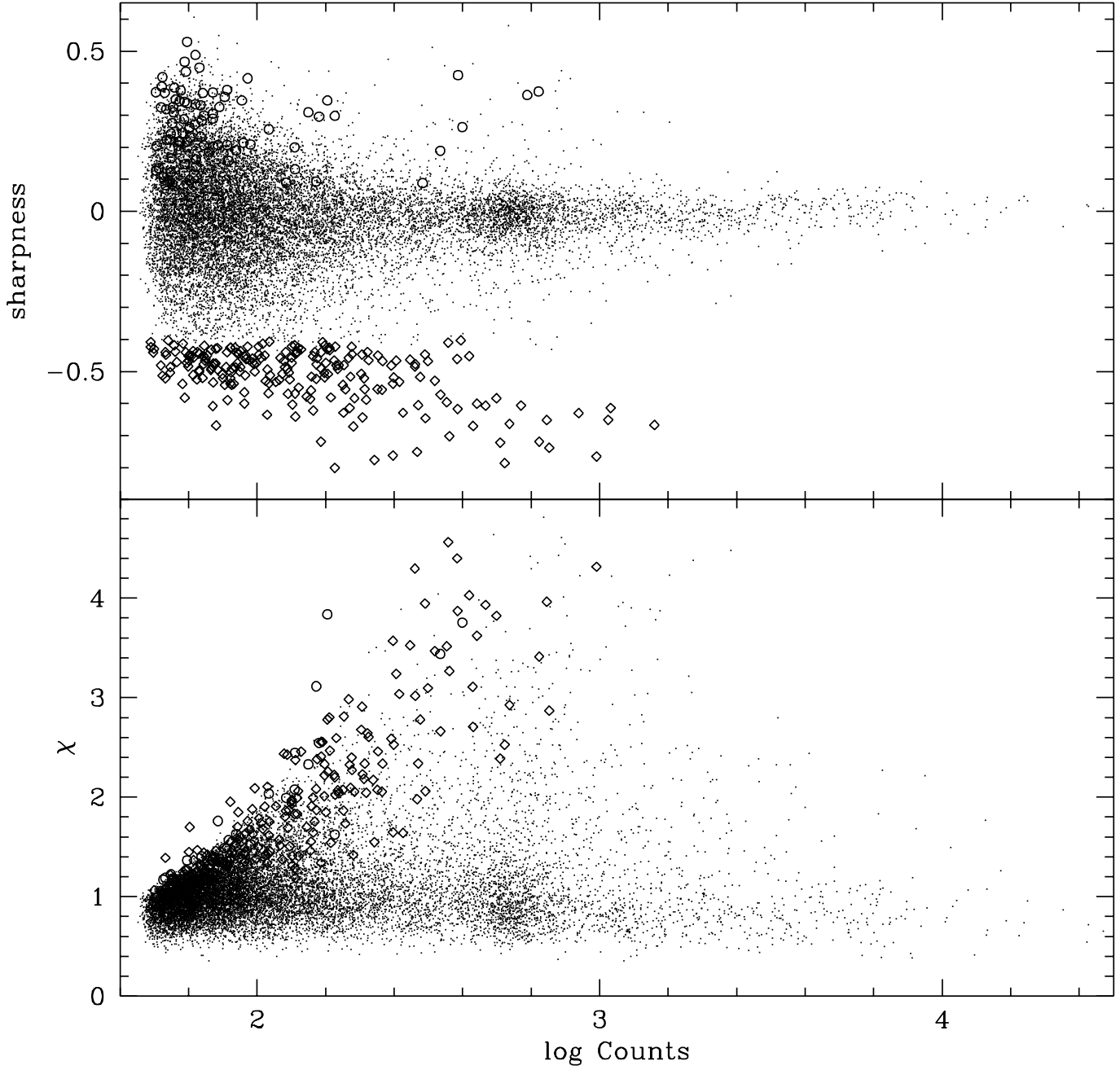


Fig. 5.— Sharpness and χ values for stars in an F555W image. HSTphot type 4 (cosmic rays) are plotted as circles; type 5 (extended objects) are plotted as diamonds.

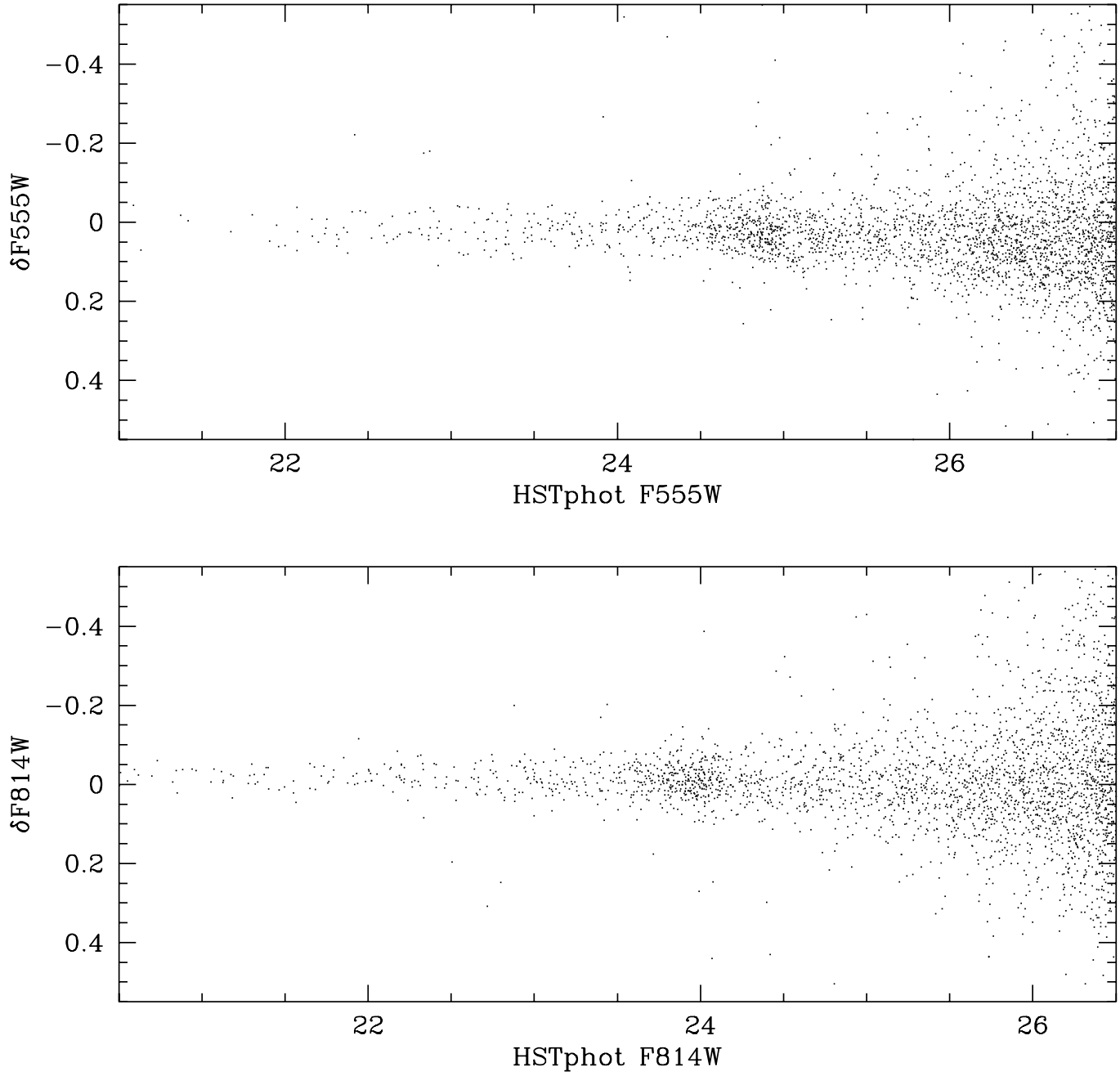


Fig. 6.— HSTphot - DoPHOT magnitudes for the WFC2 chip of an IC 1613 image

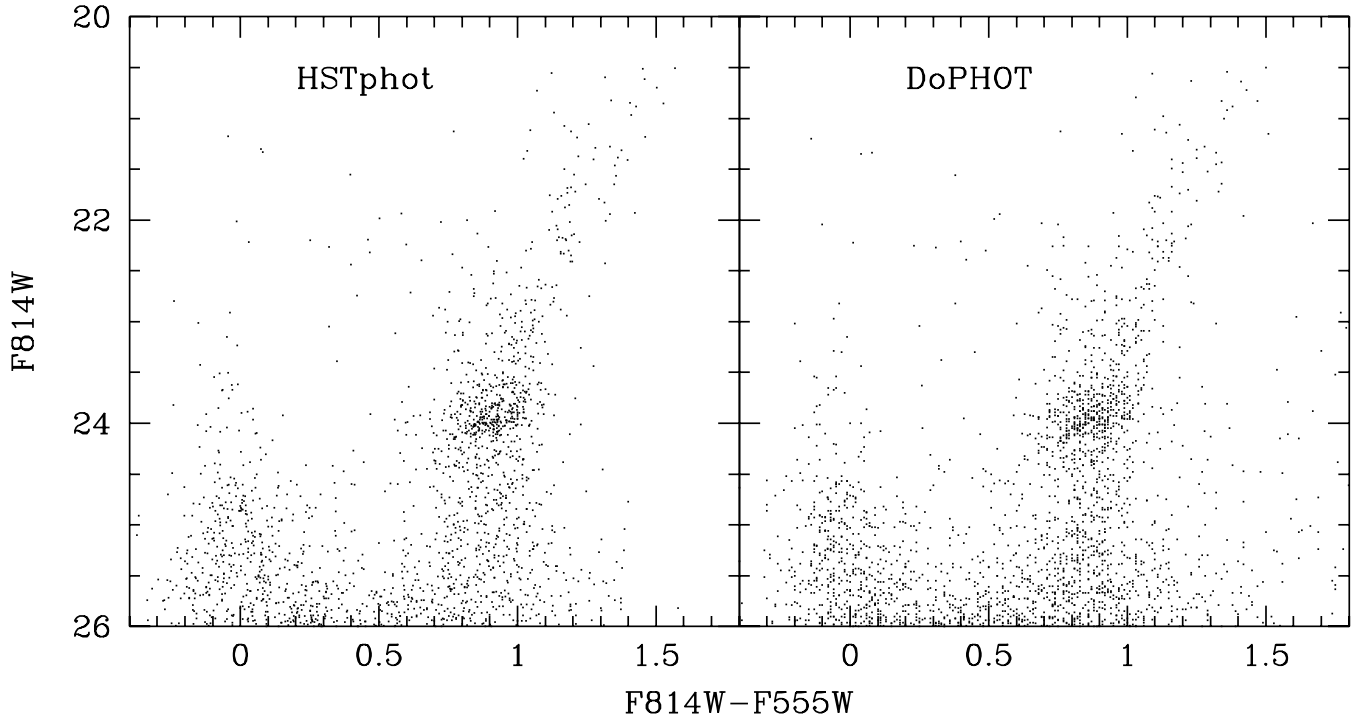


Fig. 7.— $(F555W-F814W, F814W)$ CMDs of the WFC2 chip of an IC 1613 image, as produced by HSTphot and DoPHOT

Table 1. Filter-Dependent Plate Scale Corrections

Filter	Correction ¹
F170W	45.1
F300W	7.2
F336W	4.2
F380W	4.0
F410M	2.1
F439W	1.6
F450W	1.4
F467M	0.9
F547M	-0.7
F555W	0.0
F569W	-0.8
F606W	-2.3
F622W	-2.6
F675W	-2.5
F702W	-5.2
F785LP	-4.8
F791W	-4.6
F814W	-5.0
F850LP	-5.1
F1042M	-6.2

¹Values are given in units of 10^{-4} pixels per pixel, and have typical uncertainties of 2×10^{-5}

Table 2. HSTphot-DoPHOT Photometry Comparison

Region	F814W limits	F555W-F814W limits	HSTphot F555W-F814W	DoPHOT F555W-F814W
Upper RGB	21.50 – 22.00	0.9 – 1.5	1.197 ± 0.090	1.198 ± 0.090
Red Clump	23.50 – 24.25	0.6 – 1.1	0.867 ± 0.093	0.870 ± 0.093

This figure "f1.gif" is available in "gif" format from:

<http://arxiv.org/ps/astro-ph/0006217v1>